

Scale Invariance of Graph Neural Networks

1st Qin Jiang

*School of Mathematical and Computer Sciences
Herio-Watt University
Edinburgh, UK
qj2004@hw.ac.uk*

2nd Chengjia Wang

*School of Mathematical and Computer Sciences
Herio-Watt University
Edinburgh, UK
chengjia.wang@hw.ac.uk*

3rd Michael Lones

*School of Mathematical and Computer Sciences
Herio-Watt University
Edinburgh, UK
m.lones@hw.ac.uk*

4th Wei Pang

*School of Mathematical and Computer Sciences
Herio-Watt University
Edinburgh, UK
W.Pang@hw.ac.uk*

Abstract—We address two fundamental challenges in Graph Neural Networks (GNNs): (1) the lack of theoretical support for invariance learning, a critical property in image processing, and (2) the absence of a unified model capable of excelling on both homophilic and heterophilic graph datasets. To tackle these issues, we establish and prove scale invariance in graphs, extending this key property to graph learning, and validate it through experiments on real-world datasets. Leveraging directed multi-scaled graphs and an adaptive self-loop strategy, we propose ScaleNet, a unified network architecture that achieves state-of-the-art performance across four homophilic and two heterophilic benchmark datasets. Furthermore, we show that through graph transformation based on scale invariance, uniform weights can replace computationally expensive edge weights in digraph inception networks while maintaining or improving performance. For another popular GNN approach to digraphs, we demonstrate the equivalence between Hermitian Laplacian methods and GraphSAGE with incidence normalization. ScaleNet bridges the gap between homophilic and heterophilic graph learning, offering both theoretical insights into scale invariance and practical advancements in unified graph learning. Our implementation is publicly available at <https://github.com/Qin87/ScaleNet/tree/Aug23>.

Index Terms—scale invariance, Graph Neural Network, directed graph, heterophilic graph, homophilic graph.

I. INTRODUCTION

Graph Neural Networks (GNNs) have emerged as powerful tools for learning from graph-structured data, with significant applications in node classification tasks such as protein function prediction [1], user categorization in social networks [2], Internet content recommendation [3], and document classification in citation networks [4]. Despite their proven effectiveness in node classification, GNNs face two major limitations that hinder their theoretical understanding and practical deployment.

First, from a theoretical perspective, GNNs lack robust theoretical foundations for invariant learning—a fundamental concept well-established in image classification tasks. While convolutional neural networks have well-understood invariance properties that enable robust classification regardless of image

transformations, analogous theoretical frameworks for node classification in graphs remain underdeveloped. This gap in theoretical understanding limits our ability to design and optimize GNN architectures for node classification tasks.

Second, from an empirical standpoint, existing GNN architectures demonstrate a notable dichotomy in their node classification performance: they typically excel either on homophilic graphs [5] (where connected nodes share similar labels) or heterophilic graphs [6] (where connected nodes have different labels). This dichotomy raises important questions about the underlying mechanisms that determine model effectiveness across different graph types.

To address these limitations, we make three key contributions:

- 1) We establish and prove scale invariance in graphs, extending this fundamental concept from image processing to graph learning
- 2) We develop a unified network architecture that translates this theoretical insight into practice
- 3) We introduce an adaptive self-loop strategy that dynamically adjusts to graph homophily characteristics

Our technical analysis further reveals:

- By applying graph transformation based on scale invariance, uniform weights can replace the computationally expensive edge weights in digraph inception networks, maintaining or even improving performance while reducing complexity.
- There is an equivalence between Hermitian Laplacian methods (e.g., MagNet [7]) and GraphSAGE [2] when incidence normalization is applied.

Our evaluation shows that the proposed method achieves state-of-the-art results on four homophilic and two heterophilic graphs. Compared to existing approaches, our method offers superior performance on homophilic datasets versus Dir-GNN [6], better handling of heterophilic data than MagNet [7], and improved efficiency over real symmetric Laplacian methods. Furthermore, our multi-scale graph approach provides notable

advantages for highly imbalanced datasets through implicit data augmentation.

The remainder of this paper is organized as follows:

- Section II introduces the motivation behind our work and reviews relevant research on invariant learning and higher-order neighborhood aggregation in graphs.
- The main contribution of this paper is presented across several sections. Section III defines scaled graphs and discusses the concept of scale invariance. Section IV provides a theoretical proof of scale invariance, along with experimental validation, including an analysis of self-loops. Section V introduces ScaleNet, our unified model, and Section VI presents experimental results demonstrating the performance of ScaleNet.
- Finally, Sections VII and VIII review existing GNNs for undirected and directed graphs, respectively. For directed graphs, we enhance digraph inception models by incorporating scale invariance, reducing the computational overhead of edge weights, and improving performance. We also demonstrate that Hermitian models, another popular approach for directed graphs, also suffer from unnecessary complexity and offer no fundamental advantages over simpler methods.

II. MOTIVATION AND RELATED WORK

A. Invariant Learning Techniques

Invariant classifiers generally exhibit smaller generalization errors compared to non-invariant techniques [8]. Therefore, explicitly enforcing invariance in GNNs could potentially improve their robustness and accuracy [9]. To improve the generalization ability of GNNs, in this research we focus on invariant learning techniques for node classification.

An invariant classifier [9] is less affected by specific transformations of the input than non-invariant classifiers. Invariant learning techniques have been well studied in Convolutional Neural Networks (CNNs), where they address translation, scale, and rotation invariance for image classification [10], [11].

However, the application of invariant classifiers in GNNs is less explored. The non-Euclidean nature of graphs introduces extra complexities that make it challenging to directly achieve invariance, and thus the invariance methods derived from CNNs cannot be straightforwardly applied.

B. Invariance of Graphs

In Graph Neural Networks (GNNs), two types of permutation invariance are commonly utilized:

- 1) **Global Permutation Invariance:** Across the entire graph, the output of a GNN should remain consistent regardless of the ordering of nodes in the input graph. This property is particularly useful for graph augmentation techniques [12].
- 2) **Local Permutation Invariance:** At each node, permutation-invariant aggregation functions ensure that

the results of operations remain unaffected by the order of input elements within the node’s neighborhood.

Despite these established forms of invariance, the exploration of invariance in graphs is still limited. Current research is primarily preliminary, focusing on aspects such as generalization bounds [13], [14] and permutation-invariant linear layers [15], with few advances beyond these initial investigations.

Current research on graph invariance learning techniques can be categorized into two main areas [16].

1. Invariant Graph Learning focuses on capturing stable features by minimizing empirical risks [17].

2. Graph Data Augmentation encompasses both random and non-random methods, as detailed below:

- **Random augmentation** introduces variability into graph features to improve generalization [18] and may include adversarial strategies [19]. However, excessive random augmentation can disrupt stable features and lead to uncontrolled distributions.
- **Non-Random Augmentation** involves specifically designed techniques such as graph rewiring [20] and graph reduction [21]. Graph reduction creates various perspectives of a graph through reductions at different ratios, thus augmenting the data for subsequent models. Examples include graph pooling [22], multi-scale graph coarsening [23], and using synthetic nodes to represent communities [24]. Among these, augmenting connections with high-order neighborhoods is a particularly popular technique.

C. Higher-Order Neighborhood Aggregation

Several methods extend GNNs by aggregating information from higher-order neighborhoods. These methods generally fall into two categories:

- **Type 1: Powers of the Adjacency Matrix** This approach uses powers of the adjacency matrix A^k . For example, MixHop [25] aggregates messages from multi-hop neighbors by mixing different powers of the adjacency matrix. Adaptive Diffusions [26] enhances this aggregation by sparsifying the matrix based on the landing probabilities of multi-hop neighbors. GPR-GNN [27] introduces learnable weights for features from various orders, while H2GCN [28] combines MixHop with other techniques to address disassortative graphs. Additionally, Zhang et al. [29] investigates Invariant Neighborhood Patterns to manage shifts in neighborhood distribution, integrating both high-order and low-order information.
- **Type 2: k -th Order Proximity** This method involves k -th order proximity, utilizing the multiplication of powers of the adjacency matrix A with its transpose A_t : $A^{k-1}A_t^{k-1}$. Techniques such as DiGCN(ib) [5] and SymDiGCN [30] use this approach to capture richer neighborhood information.

To the best of our knowledge, there is currently no graph data augmentation method based on invariance.

III. SCALED GRAPH

A. Scaled Ego-Graphs

Let $G = (V, E)$ be a directed graph with n nodes and m edges, represented by an adjacency matrix $A \in \{0, 1\}^{n \times n}$, where $A_{ij} = 1$ indicates the presence of a directed edge from node i to node j , and $A_{ij} = 0$ indicates the absence of such an edge. We focus on node classification where node features are organized in an $n \times d$ matrix X , where d is dimension of features and node labels are $y_i \in \{1, \dots, C\}$.

Definition 1 (In-Neighbour). An *in-neighbour* of a node $v \in V$ is a node $u \in V$ such that there is a directed edge from u to v , i.e., $(u, v) \in E$.

Definition 2 (Out-Neighbour). An *out-neighbour* of a node $v \in V$ is a node $u \in V$ such that there is a directed edge from v to u , i.e., $(v, u) \in E$.

An α -depth ego-graph [31] includes all nodes within α hops from a central node. We extend this concept to directed graphs and introduce scaled hops, leading to scaled ego-graphs.

Definition 3. In a directed graph $G = (V, E)$, we define two types of α -depth ego-graphs centered at a node $v \in V$.

- **α -depth in-edge ego-graph:** $I_\alpha(v) = (V_{\leftarrow}, E_{\leftarrow})$, where V_{\leftarrow} consists of all nodes that can reach v within α steps, and E_{\leftarrow} consists of all directed edges between nodes in V_{\leftarrow} that are within α steps of v .
- **α -depth out-edge ego-graph:** $O_\alpha(v) = (V_{\rightarrow}, E_{\rightarrow})$, where V_{\rightarrow} consists of all nodes that can be reached from v within α steps, and E_{\rightarrow} consists of all directed edges from v to nodes in V_{\rightarrow} within α steps.

As illustrated in Figure 1, a 1-depth ego-graph for an undirected graph includes nodes labeled I (in-neighbor) and O (out-neighbor). In the case of a directed graph, the 1-depth in-edge ego-graph comprises nodes labeled I along with the center node and all the edges connecting them, whereas the 1-depth out-edge ego-graph comprises nodes labeled O along with the center node and all the edges connecting them.

The 1-hop neighbour with different adjacency matrix is shown in Table I.

Adjacency Matrix	A	A^T	AA	$A^T A^T$	AA^T	$A^T A$
1-hop Neighbour	I	O	II	OO	IO	OI

TABLE I: 1-hop neighbours for GNN with different adjacency matrix

Definition 4. A **scaled-edge** is defined as an ordered sequence of multiple directed edges, where the **scale** refers to the number of edges in this sequence. Specifically, a k^{th} -**scale edge** is a scaled-edge composed of k directed edges, also referred to as a k -**order edge**.

An α -**depth scaled ego-graph** includes all nodes that are reachable within α hops of scaled-edge from a given center node.

A 1^{st} -scale edge, includes in-edge (I) and out-edge (O), connecting to in-neighbor (I) and out-neighbor (O) nodes, respectively, as shown in Figure 1. Considering a 2^{nd} -scale edge, there are four types: II, IO, OI, and OO, each connecting to nodes labeled in Figure 1 accordingly.

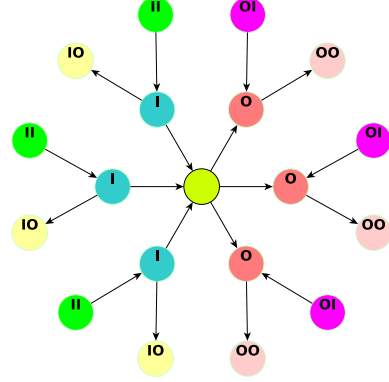


Fig. 1: An illustration of scaled ego-graphs. For directed graphs, the 1-depth in-edge ego-graph comprises nodes labeled “I” along with the center node and all in-edges between them, whereas the 1-depth out-edge ego-graph comprises nodes labeled O along with the center node and all out-edges between them. The four types of 1-depth 2^{nd} -scaled ego-graphs are composed of nodes labeled “IO”, “OI”, “II”, and “OO”, with the center node and all corresponding 2^{nd} -scaled edges between them.

B. Scale Invariance of Graphs

The concept of scale invariance, well-known in image classification as the ability to recognize objects regardless of their size, can be extended to graphs. In the context of node classification, each node to be classified can be viewed as the center of an ego-graph. Thus, for node-level prediction tasks on graphs, each input instance is essentially an ego-graph G_v centered at node v , with a corresponding target label y_v . Scale invariance in graphs would imply that the classification of a node remains consistent across different scaled ego-graphs.

Definition 5. Let S_k denote the set of all k^{th} -scale edges and $G_\alpha^k(v)$ denote the set of all α -depth k^{th} -scale ego-graphs centered at node v . Then we have the following equations:

$$S_k = \{e_1 e_2 \dots e_k \mid e_i \in \{\rightarrow, \leftarrow\}, 1 \leq i \leq k\} \quad (1)$$

$$G_\alpha^k(v) = \{(V_s, E_s) \mid s \in S_k\}, \quad (2)$$

where $e_1 e_2 \dots e_k$ represents the scaled-edge obtained by following an ordered sequence of in-edge (\leftarrow) or out-edge (\rightarrow) hops from v . Specifically:

- V_s consists of all nodes that can be reached from v within α steps of scaled-edge s .
- E_s consists of all scaled-edges s from v to these nodes within those α steps.

Consider a GNN model M that learns from a graph G using its adjacency matrix A by aggregating information solely from its out-neighbors. To also learn from the in-neighbors, the model should aggregate information from the transpose of the adjacency matrix, i.e., A^T [6].

An adjacency matrix which encodes scaled-edges is the ordered sequential multiplication of A and A^T . The graph whose structure is represented with the scaled adjacency matrix is a scaled graph.

Definition 6 (Scaled Adjacency Matrix and Scaled Graph). Let A_k denote the set of all k^{th} -scale adjacency matrix and G^k denote the set of all k^{th} -scale graphs.

$$A_k = \{a_1 a_2 \dots a_k \mid a_i \in \{A, A^T\}, 1 \leq i \leq k\} \quad (3)$$

$$G^k = \{G^k = (V, \tilde{E}_s) \mid s \in S_k\}, \quad (4)$$

where \tilde{E}_s represents pairwise connections between nodes that are k steps apart in the original graph.

To capture information from 2^{nd} -scale neighbors, the model should extend its learning to matrices that incorporate both direct and transitive relationships. This involves using matrices such as AA , AA^T , $A^T A^T$, and $A^T A$ as the scaled adjacency matrix.

Definition 7. For a node classification task on a graph G , we say the task exhibits scale invariance if the classification of a node v remains invariant across different scales of its ego-graphs. Formally, for any $k \geq 1$:

$$f(G_v) = f(G^k(v)), \quad (5)$$

where f is the classification function producing discrete values, G_v is the original ego-graph of node v , and $G^k(v)$ is any k^{th} -scale ego-graph centered at v .

This property implies that the essential structural information for node classification is preserved across different scales of the ego-graph. In other words, the k^{th} -scaled ego-graphs should maintain the node classification invariant.

IV. PROOF OF SCALE INVARIANCE

In this section, we present a proof of scale invariance for Graph Neural Networks (GNNs), exploring the relationship between standard and scaled adjacency matrices in node classification tasks. First, we derive the output of a k -layer GCN using the adjacency matrix A . We then extend this to scaled adjacency matrices with bidirectional aggregation, demonstrating that the resulting models are equivalent to dropout versions of lower-scale, bidirectional GCNs that aggregate using both A and A^T . The cases of adding self-loops and not adding them are discussed separately. We focus on the Graph Convolutional Network (GCN) model [4] as it represents the basic form of neighborhood aggregation.

A. Preliminaries

Let X denote node features, A denote the adjacency matrix (where an element is 1 if an edge exists and 0 otherwise), W

denote a general weight matrix, D denote the degree matrix of A , and I denote the identity matrix. For a scaled edge \hat{e} (as defined in Definition 4), let $X_{\hat{e}}$ represent the 1-hop neighbors of X through \hat{e} .

Theory 1. The layer-wise propagation of a GCN is:

- Without self-loops: $\sum W X_I$
- With self-loops: $\sum W X_I + W X$

Proof. As outlined in Table VI, \tilde{A} denotes incidence-normalized A , the layer-wise propagation of a GCN is:

- Without self-loops: $\tilde{A}(WX)$
- With self-loops: $(A + I)(WX)$

Since incidence normalization corresponds to a component-wise multiplication with the normalization matrix N , we have $\tilde{A}(WX) = (N \odot A)(WX)$. By the Universal Approximation Theorem, this is equivalent to WAX . Here, AX represents the aggregation of neighbor features, and thus $AX = \sum X_I$, where I represents the 1-hop in-edges. Similarly, $(A + I)(WX)$ is $\sum W X_I + W X$. \square

1) n -Layer GCN (Without Self-loops)

Theory 2. For all natural numbers n , the output of an n -layer GCN without self-loops can be expressed as:

$$X^n \approx \sum W X_{\underbrace{I \dots I}_n},$$

where $X_{\underbrace{I \dots I}_n}$ denotes neighbours reached by n -hop in-edges.

Proof. Base Case: In a 1-layer GCN, the output is expressed as:

$$X^1 = \sum W X_I,$$

which is consistent with the desired form.

For a 2-layer GCN, the output becomes:

$$X^2 = \sum W_1 \left(\sum W_2 (X_I)_I \right).$$

According to the Universal Approximation Theorem, neural networks can approximate any continuous function, given sufficient capacity and appropriately chosen weights. This theorem implies that rearranging the order of linear operations, such as:

$\sum W_1 \left(\sum W_2 (X_I)_I \right) \approx W \sum \left(\sum (X_I)_I \right) = W \sum X_{II}$, does not affect the network's ability to approximate the target function. Thus,

$$X^2 \approx \sum W X_{II}.$$

This satisfies the form for $n = 2$.

Inductive Step: Assume that the statement holds for $n = k$, i.e.,

$$X^k \approx \sum W X_{\underbrace{I \dots I}_k}.$$

For $n = k + 1$:

$$\begin{aligned} X^{k+1} &\approx (X^k)^1 \approx \sum W_1 X_I^k \approx W_1 \sum \left(W_2 \sum X_{\underbrace{I \dots I}_k} \right)_1 \\ &\approx W \sum X_{\underbrace{I \dots I}_{k+1}} \end{aligned} \quad (6)$$

Thus, the statement holds for $n = k + 1$.

Conclusion: By the principle of mathematical induction, we conclude that for all $n \geq 1$,

$$X^n \approx W \sum X_{\underbrace{I \dots I}_n}.$$

□

2) n -Layer GCN (With Self-loops)

Theory 3. For an n -layer GCN with self-loops, the output can be expressed as:

$$X^n \approx \sum W_1 X_{\underbrace{I \dots I}_n} + \sum W_2 X_{\underbrace{I \dots I}_{n-1}} + \dots + W_{n+1} X.$$

Proof. Base Case: For $n = 1$, the output of 1-layer GCN with self-loops is:

$$X^1 \approx \sum W X_1 + W X,$$

which matches the desired form.

For $n = 2$, the output is:

$$X^2 = \sum W_1 \left(\sum W_2 (X_I)_I \right) + W_3 X^1.$$

Substituting $X^1 \approx \sum W X_1 + W X$:

$$X^2 \approx \widehat{W}_1 \sum X_{II} + \widehat{W}_2 \sum X_1 + \widehat{W}_2 X.$$

This matches the desired form for $n = 2$.

Inductive Step: Assume that the statement holds for $n = k$, i.e.,

$$X^k \approx \sum W_1 X_{\underbrace{I \dots I}_k} + \sum W_2 X_{\underbrace{I \dots I}_{k-1}} + \dots + W_{k+1} X.$$

From the GCN formulation, we have:

$$\begin{aligned} X^{k+1} &= \sum \widehat{W}_1 \sum \widehat{W}_2 (X_k)_I + \widehat{W}_3 X^k \\ &\approx \widehat{W}_1 \sum X_{k+1} + \widehat{W}_3 X^k. \end{aligned}$$

Substituting the inductive hypothesis for X^k :

$$X^k \approx \sum W_1 X_{\underbrace{I \dots I}_k} + \sum W_2 X_{\underbrace{I \dots I}_{k-1}} + \dots + W_{k+1} X.$$

Thus:

$$\begin{aligned} X^{k+1} &\approx \sum W_1 X_{k+1} + \sum W_2 X_k + \\ &\quad \sum W_3 X_{k-1} + \dots + \sum W_{k+1} X_1 + W_{k+2} X. \end{aligned} \quad (7)$$

Conclusion: By the principle of mathematical induction, the statement holds for all $n \geq 1$:

$$X^n \approx \sum W_1 X_{\underbrace{I \dots I}_n} + \sum W_2 X_{\underbrace{I \dots I}_{n-1}} + \dots + W_{n+1} X.$$

□

Next, we will prove a fundamental property of GNNs for directed graphs: scale invariance. We will demonstrate that when the input graph undergoes scaling transformations, the GCN's output remains unchanged, considering both scenarios—whether or not self-loops are added. This proof highlights that the GNN's architecture inherently preserves its effectiveness and consistency across scaled graph representations, ensuring robust performance in diverse scenarios.

B. Proof of Scale Invariance in GCN without Self-loops

For different adjacency matrices, the layer-wise propagation rules are as follows:

1) Single-Directional Aggregation

- A as adjacency matrix:
 - 1 layer: $\sum W X_I$
 - k layer: $\sum W X_{\underbrace{I \dots I}_k}$
- A^T as adjacency matrix:
 - 1 layer: $\sum W X_O$
 - k layer: $\sum W X_{\underbrace{O \dots O}_k}$
- AA as adjacency matrix:
 - 1 layer: $\sum W X_{II}$
 - k layer: $\sum W X_{\underbrace{I \dots I}_{2k}}$
- AA^T as adjacency matrix:
 - 1 layer: $\sum W X_{IO}$
 - k layer: $\sum W X_{\underbrace{IO \dots IO}_{k \text{ pairs } IO}}$

[Similar patterns for $A^T A^T$ and $A^T A$]

From above, we can deduce:

- 1) k -layer GCN with AA is equivalent to $2k$ -layer GCN with A
- 2) k -layer GCN with $A^T A^T$ is equivalent to $2k$ -layer GCN with A^T

2) Bidirectional Aggregation

If the model uses bidirectional aggregation [6], the layer-wise propagation rules are as follows:

- A and A^T as adjacency matrix:
 - 1 layer: $\sum W_0 X_I + \sum W_1 X_O$
 - k layer: $\sum W_0 X_{\underbrace{II \dots I}_k} + \sum W_1 X_{\underbrace{OI \dots I}_k} + \dots + \sum W_k X_{\underbrace{O \dots O}_k}$
- AA^T and $A^T A$ as adjacency matrix:
 - 1 layer: $\sum W_0 X_{IO} + \sum W_1 X_{OI}$
 - k layer: $\sum W_0 X_{\underbrace{IO \dots IO}_{k \text{ pairs } IO}} + \dots + \sum W_k X_{\underbrace{OI \dots OI}_{k \text{ pairs } OI}}$

[Similar patterns for AA and $A^T A^T$]

From the above, we can deduce:

- 1) A k -layer GCN with AA^T and $A^T A$ is a dropout version of a $2k$ -layer GCN with A and A^T .
- 2) A k -layer GCN with AA and $A^T A^T$ is also a dropout version of a $2k$ -layer GCN with A and A^T .

Synthesizing Section IV-B1 and Section IV-B2, we conclude that all single-directional aggregation models are dropout versions of their bidirectional counterparts. For example, a model using only A corresponds to a bidirectional model with both A and A^T , and a model using AA corresponds to a bidirectional model with both AA and $A^T A^T$.

Finally, we can conclude that all models—whether single-directional or bidirectional—are dropout versions of A and A^T .

C. Proof of Scale Invariance of GCN with Self-loops

Similarly, cases of GCN which adds self-loops are as follows:

1) Single-Directional Aggregation

- A as adjacency matrix
 1 layer: $\sum W_0 X_I + W_1 X$
 k layer: $\sum W_0 X_{\underbrace{I \dots I}_k} + \sum W_1 X_{\underbrace{I \dots I}_{k-1}} + \dots + W_k X$
- A^T as adjacency matrix
 1 layer: $\sum W_0 X_O + W_1 X$
 k layer: $\sum W_0 X_{\underbrace{O \dots O}_k} + \sum W_1 X_{\underbrace{O \dots O}_{k-1}} + \dots + W_k X$
- AA as adjacency matrix
 1 layer: $\sum W_0 X_{II} + W_1 X$
 k layer: $\sum W_0 X_{\underbrace{I \dots I}_{2k}} + \sum W_1 X_{\underbrace{I \dots I}_{2(k-1)}} + \dots + \sum W_{k-1} X_{II} + W_k X$
- AA^T as adjacency matrix
 1 layer: $\sum W_0 X_{IO} + W_1 X$
 k layer: $\sum W_0 X_{\underbrace{IO \dots IO}_{k \text{ times IO}}} + \sum W_1 X_{\underbrace{IO \dots IO}_{k-1 \text{ times IO}}} + \dots + \sum W_{k-1} X_{IO} + W_k X$

[Similar patterns for $A^T A^T$ and $A^T A$]

From above, we can deduce that:

- 1) k layer AA is equivalent of dropout of $2k$ layer A .
- 2) k layer $A^T A^T$ is equivalent of dropout of $2k$ layer A^T .

2) Bi-Directional Aggregation

- A and A^T as adjacency matrix
 1 layer: $\sum W_0 X_I + \sum W_1 X_O + W_2 X$
 k layer: $\sum W_{k_0} X_{\underbrace{II \dots I}_k} + \sum W_{k_1} X_{\underbrace{OI \dots I}_k} + \dots + \sum W_{k_k} X_{\underbrace{O \dots O}_k} + \dots + \sum W_{1_0} X_I + \sum W_{1_1} X_O + W_0 X$
- AA and $A^T A^T$ as adjacency matrix
 1 layer: $\sum W_0 X_{II} + \sum W_1 X_{OO} + W_2 X$
 k layer: $\sum W_{k_0} X_{\underbrace{II \dots II}_{k \text{ pairs II}}} + \sum W_{k_1} X_{\underbrace{OOII \dots II}_{k \text{ pairs II or OO}}} + \dots +$

$$\sum W_{k_k} X_{\underbrace{OO \dots OO}_{k \text{ pairs OO}}} + \dots + \sum W_{1_0} X_{II} + \sum W_{1_1} X_{OO} + W_0 X$$

- AA^T and $A^T A$ as adjacency matrix
 1 layer: $\sum W_0 X_{IO} + \sum W_1 X_{OI} + W_2 X$
 k layer: $\sum W_{k_0} X_{\underbrace{IO \dots IO}_{k \text{ pairs IO}}} + \sum W_{k_1} X_{\underbrace{OIIO \dots IO}_{k \text{ pairs IO or OI}}} + \dots + \sum W_{k_k} X_{\underbrace{OI \dots OI}_{k \text{ pairs OI}}} + \dots + \sum W_{1_0} X_{IO} + \sum W_{1_1} X_{OI} + W_0 X$

From above, we can deduce that:

- 1) k layer $AA + A^T A^T$ is equivalent of dropout of $2k$ layer A and A^T .
- 2) k layer $AA^T + A^T A$ is equivalent of dropout of $2k$ layer A and A^T .

In conclusion, our theoretical analysis confirms that propagating information through higher-scale adjacency matrices is fundamentally equivalent to applying lower-scale graph operations or their dropout variants. This equivalence not only supports the theoretical validity of scale invariance in graph neural networks but also ensures that the use of multi-scale graphs retains the benefits of invariance across different graph structures.

Furthermore, as undirected graphs can be treated as a special case of directed graphs, where in-neighbors and out-neighbors are identical, the proof of scale invariance extends seamlessly to undirected graph structures. These findings provide a solid foundation for developing more efficient and scalable graph neural network models that leverage multi-scale graph representations.

While we demonstrate the proof of scale invariance specifically for GCN, similar mathematical arguments can be constructed for GraphSAGE and other GNN variants. These findings provide a solid foundation for developing more efficient and scalable graph neural network models that leverage multi-scale graph representations.

D. Empirical Demonstration of Scale Invariance

In Table II, we demonstrate the presence of scale invariance in graphs through various experiments. We represent the graph structure using a scaled adjacency matrix, which is then fed into a GNN for node classification. The results in Table II show that higher-scale graphs consistently achieve performance comparable to their lower-scale counterparts, confirming scale invariance. In contrast, if scale invariance were absent, the performance of higher-scale graphs would be similar to the results shown in the last column, where no input is provided.

Additionally, combinations of ego-graphs with adverse directional edges tend to yield better results than the individual ego-graphs. For example, $AA^T + A^T A$ generally achieves better accuracy compared to AA^T and $A^T A$ individually, and $AA + A^T A^T$ performs better than AA and $A^T A^T$.

For heterophilic graphs like Chameleon and Squirrel:

Type	Dataset	A	A^T	$A+A^T$	AA^T	$A^T A$	$AA+A^T A$	AA	$A^T A^T$	$AA+A^T A^T$	None
Homophilic	Telegram	68	74	100	60 (58)	68 (78)	92 (94)	72 (50)	80 (78)	92 (92)	38
	Cora-ML	75	70	78	78 (73)	77 (69)	79 (78)	75 (80)	72 (78)	77 (79)	29
	CiteSeer	56	59	62	62 (57)	64 (59)	63 (61)	57 (53)	60 (60)	63 (63)	20
	WikiCS	73	66	75	74 (76)	65 (69)	76 (78)	73 (75)	66 (67)	73 (77)	23
Heterophilic	Chameleon	78	30	68	66 (70)	29 (29)	68 (71)	70 (76)	30 (31)	66 (69)	22
	Squirrel	75	33	68	73 (73)	31 (31)	70 (67)	75 (73)	32 (33)	66 (66)	19

TABLE II: Accuracy obtained by each scaled ego-graph using a single split per ego-graph. Higher scaled graphs maintain the discerning ability of their lower scale counterparts, even after removing the shared edges from lower scale graphs (in parentheses). For homophilic graphs, both A and A^T perform well, and all 2^{nd} -scale graphs preserve this performance. In heterophilic graphs, A performs well while A^T does not. AA and AA^T preserve the performance of A , whereas $A^T A^T$ and $A^T A$ inherit the poor performance of A^T . (The final column presents the performance with all zero input for comparison. The value in parentheses is the scaled graph after removing the shared edges with A or A^T . “+” denotes the addition of aggregation outputs.)

Dataset	Direction	Homo.	Hetero.	No Neigh.
Chameleon	A	576	1701	0
	A^T	237	627	1413
Squirrel	A	1258	3943	0
	A^T	441	1764	2996

TABLE III: This figure illustrates the distribution of nodes in the Chameleon and Squirrel datasets, categorized by the predominant label of their aggregated neighbors in relation to the node’s own label. The analysis reveals that when using A^T as the adjacency matrix, a majority of nodes have zero aggregated neighbors. This lack of connectivity results in poor model performance

- A outperforms A^T in classification tasks. This means aggregating information from out-neighbors works better than from in-neighbors for these datasets.
- This trend extends to higher-order relationships: AA^T and AA perform better than $A^T A$ and $A^T A^T$. This suggests mutual out-neighbors or 2-hop out-neighbors capture similarity more effectively than their in-neighbor counterparts.
- The reason: Most nodes have 0 neighbors when using A^T . After aggregation, these nodes’ features are updated to all zeros.

Overall, Table II demonstrates that higher-scale graphs consistently perform no worse than their lower-scale counterparts, confirming the scale invariance of graph structures. The table also provides insights into how performance varies with different graph scales and characteristics across datasets.

E. Influence of Adding Self-loops

Adding self-loops is traditionally understood as assigning the highest weight to a node itself. However, in this paper, we highlight that adding self-loops also facilitates the incorporation of multi-scale information into the graph representation.

Given an adjacency matrix A , the modified adjacency matrix

\hat{A} with self-loops is defined as:

$$\hat{A} = A + I,$$

where I is the identity matrix. The resulting products involving \hat{A} are as follows:

- $\hat{A}\hat{A}^T$:

$$\hat{A}\hat{A}^T = (A + I)(A^T + I) = AA^T + A + A^T + I$$

- $\hat{A}^T\hat{A}$:

$$\hat{A}^T\hat{A} = (A^T + I)(A + I) = A^T A + A + A^T + I$$

- $\hat{A}\hat{A}$:

$$\hat{A}\hat{A} = (A + I)(A + I) = AA + 2A + I$$

- $\hat{A}^T\hat{A}^T$:

$$\hat{A}^T\hat{A}^T = (A^T + I)(A^T + I) = A^T A^T + 2A^T + I$$

The influence of adding self-loops can be analyzed at two levels:

- 1) **Layer-wise Influence** Adding self-loops to A results in an augmented adjacency matrix, $A + I$, that incorporates all the original directed edges and self-loops. As a result, the propagation of a 1-layer GCN using AA as the adjacency matrix will, after adding self-loops, become $(A + I)(A + I)$, include not only the information from AA but also direct contributions from A and the self-loops in its output.

Since heterophilic graphs connect different types of nodes, adding self-loops dilutes this important difference-based structure. This can reduce model performance in tasks requiring heterophilic relationship learning.

- 2) **Multi-layer Influence** For a 2-layer GCN, omitting the non-linear activation for simplicity, the propagation outputs are¹:

- **Without self-loops:**

$$\tilde{A}(W_1\tilde{A}(W_2X)) \approx \tilde{A}^2(WX) = D^{-\frac{1}{2}}A^2D^{-\frac{1}{2}}(WX)$$

¹Here, \approx reflects the approximation aligned with the Universal Approximation Theory (UAT).

- **With self-loops:**

$$\begin{aligned} \widetilde{(A+I)}(W_1\widetilde{(A+I)}(W_2X)) &\approx \widetilde{(A+I)}^2(WX) \\ &= D^{-\frac{1}{2}}(AA+2A+I)D^{-\frac{1}{2}}(WX) \end{aligned}$$

Consequently, for a k -layer GCN, adding self-loops enables the network to aggregate information from k -hop neighbors, $(k-1)$ -hop neighbors, ..., 1-hop neighbors, and the node itself. In contrast, a k -layer GCN without self-loops aggregates information strictly from k -hop neighbors.

Adding self-loops enhances the propagation mechanism, facilitating the incorporation of multi-scale information. This can boost performance on homophilic datasets, where nodes with similar features are more likely to be connected. However, on heterophilic datasets, where nodes with dissimilar features tend to be connected, adding self-loops may degrade performance. Therefore, it is essential to treat the inclusion of self-loops as a dataset-specific strategy, optimizing it based on the characteristics of the data to achieve the best performance when building our models.

V. SCALENET

A. A Unified Network: ScaleNet

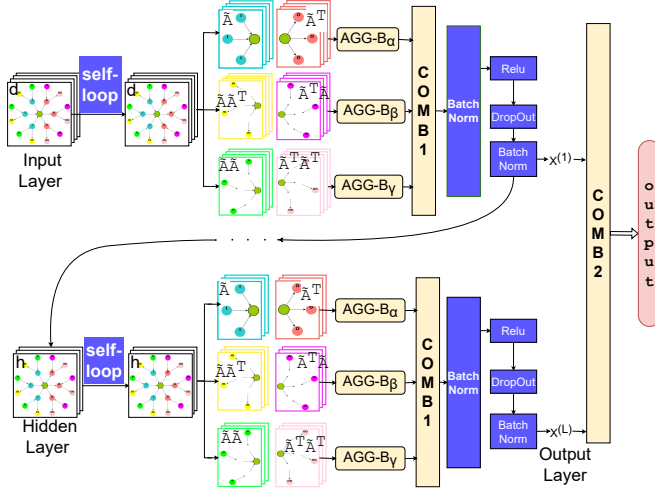


Fig. 2: Schematic depiction of multi-layer ScaleNet with d input channels and h hidden channels. For layer-wise aggregation, the original graph is derived into two 1^{st} -scaled and four 2^{nd} -scaled graphs. Three **AGG-B** blocks determine input selection for **COMB1**, which uses either a jumping knowledge architecture or addition. **COMB2** represents the fusion of all layers' outputs. (The blue blocks are optional, including self-loop operations, non-linear activation functions, dropout, and layer normalization.)

As discussed in Section IV-D, heterophilic graphs tend to suffer from performance degradation when aggregating information from scaled graphs in both directions. This limitation

causes existing Digraph Inception Networks to perform poorly on heterophilic graphs.

To address this issue and accommodate the unique characteristics of different datasets, we propose a flexible combination approach and introduce **ScaleNet**, as illustrated in Figure 2. This approach flexibly synthesizes scaled graphs and optionally integrates components like self-loops, batch normalization, and non-linear activation functions, each of which is tailored to the specific characteristics of the dataset through a grid search of model parameters.

a) Bidirectional Aggregation

To exploit scale invariance, we define the bidirectional aggregation function $\mathbf{AGG-B}_\alpha(M, N, X)$ as follows:

$$(1 + \alpha)\alpha \mathbf{AGG}(M, X) + (1 + \alpha)(1 - \alpha) \mathbf{AGG}(N, X) \quad (8)$$

The **AGG** function can be any message-passing neural network (MPNN) architecture, such as GCN [4], GAT [32], or SAGE [2]. M and N represent pairs of matrices encoding opposite directional edges. The parameter α controls the contribution of matrices M and N : $\alpha = 0$ uses only M , $\alpha = 1$ uses only N , $\alpha = 0.5$ balances both, and $\alpha = -1$ excludes both.

Given that adding or removing self-loops [4], [5] can influence the performance of the model, we allow for the inclusion of such options by defining \tilde{A} , which can be: (i) the matrix A with self-loops being removed, (ii) the matrix A with self-loops being added, or (iii) the original matrix A . The influence of self-loops is shown in Appendix IV-E.

This formulation provides a flexible framework for aggregating information from bidirectional matrices, enabling the model to leverage various directional and self-loop configurations to enhance its performance.

Additionally, setting $\alpha = 2$ combines the matrices M and N directly before aggregation, while setting $\alpha = 3$ considers their intersection:

$$\mathbf{AGG-B}_2(M, N, X) = \mathbf{AGG}(M \cup N, X) \quad (9)$$

$$\mathbf{AGG-B}_3(M, N, X) = \mathbf{AGG}(M \cap N, X) \quad (10)$$

b) Layer-wise Aggregation of ScaleNet

We combine the propagation output from various scaled graphs with the following rule:

$$X^{(l)} = \mathbf{COMB1}(X_1^{(l)}, X_2^{(l)}, X_3^{(l)}, \dots), \quad (11)$$

where $X^{(l)}$ represents the updated features after l layers. The function **COMB1** can be realized by the Jumping Knowledge (JK) framework as proposed by Xu et al. [33], or simply by performing an element-wise addition of the inputs.

c) Multi-layer ScaleNet

A multi-layer ScaleNet is then defined as follows:

$$\mathbf{Z} = \mathbf{COMB2}(X^{(1)}, X^{(2)}, \dots, X^{(L)}) \quad (12)$$

In this formulation, L layers of the propagation rule are stacked. The function **COMB2** combines the outputs of all layers, which can again be done using the Jumping Knowledge technique, or alternatively, the output from the final layer may be used directly as the model's output.

VI. EXPERIMENTS

A. Performance of ScaleNet on Different Graphs

ScaleNet is designed to adapt to the unique characteristics of each dataset, delivering optimal performance on both homophilic and heterophilic graphs. This is achieved through customizable options such as combining directed scaled graphs, incorporating batch normalization, and adding or removing self-loops.

During hyperparameter tuning via grid search, we observed the following key findings:

- **Homophilic Graphs:** Performance improves with the addition of self-loops and the use of scaled graphs derived from opposite directed scaled edges, such as AA and $A^T A^T$.
- **Heterophilic Graphs:** Performance benefits from removing self-loops and utilizing scaled graphs with preferred directional scaled edges, while excluding those based on the opposite directional scaled edges.
- Additional findings:
 - For imbalanced datasets such as the Telegram, incorporating batch normalization significantly improves performance.
 - The CiteSeer dataset performs better with the removal of nonlinear activation functions.

Our unified model, optimized through grid search, reveals the characteristics of different graph datasets and provides a strong basis for model comparison.

Table IV summarizes the 10-split cross-validation results. ScaleNet consistently achieves top performance across all six datasets, significantly outperforming existing models on both homophilic and heterophilic graphs.

B. Robustness to Imbalanced Graphs

ScaleNet improves robustness against imbalanced graphs by leveraging multi-scale graphs, similar to data augmentation techniques.

Table V indicates that ScaleNet consistently outperforms Dir-GNN and MagNet on imbalanced datasets. The imbalance ratio measures the size disparity between the largest and smallest classes. ScaleNet’s advantage stems from its use of higher-scale graphs and self-loops, which enhances its ability to capture essential features in homophilic graphs that Dir-GNN and MagNet might miss. Conversely, single-scale networks like Dir-GNN [6] and MagNet [7] are prone to incorporate irrelevant nodes due to excessive layer stacking when aggregating information from longer-range nodes.

VII. REVIEW OF GNNs

Graph Neural Networks (GNNs) operate as Message Passing Neural Networks (MPNNs), regardless of their spectral or spatial categorization. While spectral methods theoretically focus on graph spectra, they face limitations in handling feature

variations. Their success stems from effectively functioning as spatial methods in practice.

GNNs extend MLPs by adding a message passing sub-layer before the linear transformation and activation. Let X denote node features, A denote the adjacency matrix, \hat{A} denote normalized A , W denote the weight matrix, and I denote the identity matrix. Different GNN architectures primarily vary in their message passing mechanisms. In this paper, non-linear activation is omitted for simplicity. Table VI lists the message passing filters for these architectures.

- 1) GCN Graph Convolutional Network (GCN) [4] aggregates and normalizes neighbor information. \tilde{A} denotes incidence-normalized A .
- 2) SAGE GraphSAGE [2] concatenates self-node with its neighbors: Note that adding self-loops does not affect SAGE’s output. While SAGE can assign different weights to self-nodes and neighbor nodes, making it potentially more expressive than GCN, it lacks incidence normalization [4]. This can lead to performance degradation when high-degree nodes receive disproportionate weights.
- 3) ChebNet ChebNet [36] is typically recognized as a spectral method, which uses Chebyshev polynomials of the normalized Graph Laplacian $\tilde{L} = I - \tilde{A}$, following:

$$T_{k+2} = 2\tilde{L}T_{k+1} - T_k = 2(I - \tilde{A})T_{k+1} - T_k, \quad (13)$$

where $T_1 = I$ and $T_2 = I - \tilde{A}$. By combining these polynomials with learnable weights ($\sum_{i=1}^k W_i T_i X$), ChebNet effectively aggregates information from k -hop neighborhoods, making it functionally equivalent to a spatial method despite its spectral formulation.

VIII. LIMITATIONS OF EXISTING GNNs FOR DIRECTED GRAPHS

The GNN models reviewed in Section VII focus on undirected graphs. In this section, we examine GNN architectures specifically designed for directed graphs.

While traditional GNNs excel at processing undirected graphs, many real-world applications involve directed graphs where edge directionality carries crucial semantic meaning. Recent research has produced three main approaches to extending GNNs to directed graphs:

- 1) **Real Symmetric Laplacians:** These methods convert directed graphs into symmetric representations. MotifNet [37] constructs a symmetric adjacency matrix based on motifs, though this approach is constrained by the need for predefined templates and struggles with complex structures. DGCN [38], SymDiGCN [30], and DiGCN [5] address this by incorporating both the asymmetric adjacency matrix and its transpose through Markov processes. However, these methods are computationally intensive [39], limiting their scalability to large graphs.
- 2) **Hermitian Laplacians:** These methods utilize complex-valued entries in Hermitian matrices to encode directional information while retaining positive semi-definite

Type	Method	Telegram	Cora-ML	CiteSeer	WikiCS	Chameleon	Squirrel
Base models	MLP	32.8±5.4	67.3±2.3	54.5±2.3	73.4±0.6	40.3±5.8	28.7±4.0
	GCN	86.0±4.5	81.2±1.4	65.8±2.3	78.8±0.4	64.8±2.2	46.3±1.9
	APPNP	67.3±3.0	81.8±1.3	65.9±1.6	77.6±0.6	38.7±2.4	27.0±1.5
	ChebNet	83.0±3.8	80.5±1.6	66.5±1.8	76.9±0.9	58.3±2.4	38.5±1.4
	SAGE	74.0±7.0	81.7±1.2	66.7±1.7	79.3±0.4	63.4±3.0	44.6±1.3
Hermitian	MagNet	87.6±2.9	79.7±2.3	66.5±2.0	74.7±0.6	58.2±2.9	39.0±1.9
	SigMaNet	86.9±6.2	71.7±3.3	44.9±3.1	71.4±0.7	64.1±1.6	OOM
	QuaNet	85.6±6.0	26.3±3.5	30.2±3.0	55.2±1.9	38.8±2.9	OOM
Symmetric	Sym	87.2±3.7	81.9±1.6	65.8±2.3	OOM	57.8±3.0	38.1±1.4
	DiG	82.0±3.1	78.4±0.9	63.8±2.0	77.1±1.0	50.4±2.1	39.2±1.8
	DiGib	64.1±7.0	77.5±1.9	60.3±1.5	78.3±0.7	52.2±3.7	37.7±1.5
Symmetric (Ours)	1ym	84.0±3.9	80.8±1.6	64.9±2.5	75.4±0.4	54.9±2.7	35.5±1.1
	1iG	<u>95.8±3.5</u>	82.0±1.3	65.5±2.4	77.4±0.6	70.2±1.6	50.7±5.8
	1iGi2	93.0±5.1	81.7±1.3	67.9±2.2	78.9±0.6	58.4±2.5	42.7±2.5
	1iGu2	92.6±4.9	<u>82.1±1.2</u>	67.6±1.8	75.6±0.9	60.4±2.4	40.4±1.8
BiDirection	Dir-GNN	90.2±4.8	79.2±2.1	61.6±2.6	77.2±0.8	<u>79.7±1.3</u>	<u>75.3±1.9</u>
Ours	ScaleNet	96.8±2.1	82.3±1.1	68.3±1.5	79.3±0.6	80.1±1.5	76.0±2.0
	loop_α, β, γ	1_0.5,-1,-1	1_2,-1,-1	1_0.5,2,-1	1_0.5,2,-1	0_1,1,1	0_1,1,1

TABLE IV: Node classification Accuracy (%). The best results are in **bold** and the second best are underlined. 10-fold cross validation is used. OOM indicates out of memory on GPU3090 with 24GB of VRAM. Model 1ym assigns 1 to edge weights of model Sym: similarly, model 1iG and 1iGi2 are assigning 1 to edge weights of models DiG and DiGib, respectively. Model 1iGu2 and 1iGu3 assign weights of 1 to scaled edges, but use union instead of intersection in DiGib, and the last number k denotes the model includes up to k^{th} -scale edges, while DiGib only scales up to 2^{nd} -order. At the end of model name, “ib” would be used interchangeably with “i2”. Parameters α , β , and γ controlling ScaleNet components: α controls A and A^T , β controls AA^T and $A^T A$, and γ controls AA and $A^T A^T$. Parameter loop is 1 when adding selfloop and 0 when not adding.

Type	Method	Cora-ML	CiteSeer	WikiCS
Standard	MagNet	47.9±5.5	29.3	62.0±1.5
	Dir-GNN	41.1	25.0	62.9±1.4
Augment	DiG	60.9±1.8	36.9	72.2±1.4
	DiGib	55.7±2.9	40.4	69.8±1.2
	1iG	64.9±4.7	42.3	71.0±1.5
	1iGi2	61.9±5.7	41.5	71.0±1.6
	ScaleNet	60.3±6.7	43.1	69.4±1.2

TABLE V: Accuracy on imbalanced datasets (imbalance ratio = 100:1). When accuracy is below 45%, only one split is used.

eigenvalues. MagNet [7] uses Hermitian matrices with complex numbers for this purpose. Extensions to signed digraphs include SigMaNet [40] and MSGNN [41]. QuaNet [42] introduced Quaternion-valued Laplacians to capture asymmetric weights in signed directed graphs.

- Bidirectional Spatial Methods:** Recent advancements, exemplified by Dir-GNN [6], process in-neighbors and out-neighbors separately to capture directional information. Similar approaches are explored in [43]. This approach demonstrates notable improvements on heterophilic graphs but is somewhat less effective on homophilic graphs.

Current approaches to handling directed graphs with GNNs face several fundamental limitations. While the suboptimal performance of bidirectional models on homophilic graphs has been acknowledged in the seminal work [6], we identify and analyze two critical issues with other leading approaches:

- Digraph Inception Models:** While these models employ

real symmetric adjacency matrices, their computationally expensive edge weight calculations [5] provide minimal benefit. We demonstrate that simpler uniform weights can achieve comparable or superior performance.

- Hermitian Laplacian Models:** Despite their mathematical elegance, we prove that these models are functionally equivalent to GraphSAGE [2] with incidence-normalized [4] adjacency matrices, offering no fundamental advantages over simpler approaches.

A. Digraph Inception Networks

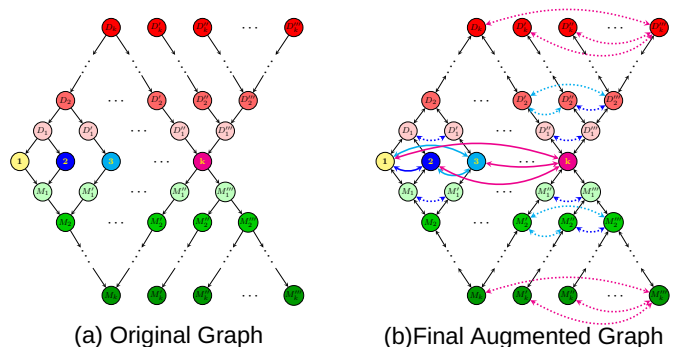


Fig. 3: Edge augmentation by stacking multi-scale graphs in Digraph Inception Model.

State-of-the-art GNNs for homophilic graphs include Di-

Model	Configuration	Layer-wise Propagation Output
MLP [34]		WX
GCN	No SelfLoop	$\tilde{A}WX$
	Add SelfLoop	$(\tilde{I} + \tilde{A})WX$
SAGE	No SelfLoop	$W_1AX + W_2X$
	Add SelfLoop	$W_1(I + A)X + W_2X$
GAT [32]	Learned edge weights W_{att} for each neighbour	
	No SelfLoop	$(W_{att} \odot A)WX$
	Add SelfLoop	$(W_{att} \odot (A + I))WX$
ChebNet	Recurrence Formula: $T_1(A) = I, T_2(A) = I - \tilde{A}, T_{k+2}(A) = 2\tilde{A}T_{k+1}(A) - T_k(A)$	
	K=1	$WT_1(A)X = WX$
	K=2	$W_1X + W_2(I - \tilde{A})X$
	K=k	$W_1X + W_2(I - \tilde{A})X + \dots + W_kT_k(A)X$
APPNP [35]	Recurrence Formula: $P_{k+1} = (1 - \alpha)\tilde{A}P_k + \alpha WX$	
	K=1(No Selfloop)	$P_1 = (1 - \alpha)AW_1X + \alpha W_2X$
	K=2(No Selfloop)	$P_2 = (1 - \alpha)\tilde{A}P_1 + \alpha W_3X =$ $(1 - \alpha)^2(\tilde{A})^2W_1X + (1 - \alpha)\alpha\tilde{A}W_2X + \alpha W_3X$
	K=k(No Selfloop)	$P_k = ((1 - \alpha)\tilde{A})^k W_1X + ((1 - \alpha)\tilde{A})^{(k-1)}\alpha W_2X + \dots + ((1 - \alpha)\tilde{A})^2\alpha W_{k-1}X +$ $((1 - \alpha)\tilde{A})\alpha W_kX + \alpha W_{k+1}X$
	Add Selfloop	replace \tilde{A} with $(\tilde{I} + \tilde{A})$ in P_k

TABLE VI: Different message passing filters of GNNs. \odot denote element-wise multiplication.

graph Inception Networks such as DiGCN(ib)² [5] and SymDiGCN [30], which use higher-order proximity for multi-scale features. However, their reliance on random walks makes edge weights across scales crucial. DiGCN(ib) requires computationally expensive eigenvalue decomposition to determine these weights, whereas SymDiGCN relies on costly node-wise outer product computations. These computational requirements pose significant scalability challenges, particularly for large-scale graph applications.

Their success stems from edge augmentation through various proximities, as shown in Figure 3.

1) Undesirable Edge Weights by DiGCN(ib)

Model	No BN	BN	Model	No BN	BN
DiG	67.4±8.1	63.0±7.6	DiGib	68.4±6.2	77.4±5.1
liG	86.0±3.4	95.8±3.5	liGib	86.2±3.2	94.2±2.7
RiG	85.2±2.5	91.0±6.3	RiGib	86.4±6.2	86.4±6.6

TABLE VII: Performance of Inception models on the Telegram dataset. “BN” indicates the addition of batch normalization to the original model. The **RiG**(ib) model assigns random weights in uniform distribution to edges within the range [0.0001, 10000], and The **liG**(ib) model assigns weight 1 to all scaled edges.

Instead of computing edge weights for higher-scaled edges, we apply the concept of scale invariance. This allows us to generate higher-scaled graphs via transformation, where the edge weights are uniform. Consequently, we replace the edge

²In this paper, DiGCN interchangeably with DiG, DiGCNib interchangeably with DiGib, DiGi2

weights in DiGCN(ib) with uniform weights of **1**, resulting in our simplified models (**liG**, **liGi2**).

We show that the computational cost associated with DiGCN(ib)’s edge weights is unnecessary, as replacing them with uniform weights of **1** still yields competitive results. The results in Table IV demonstrate that our simplified models (**liG**, **liGi2**, **lym**) either outperform or match their more complex counterparts (**DiG**, **DiGib**, **Sym**) across all datasets. Further experiments with random weights (**RiG**(i2)) in range [0.0001, 10000] show even random weighting outperforms DiGCN(ib) (Table VII), both with and without batch normalization. Additionally, Tables IV and V show **Sym** and **DiG** face memory limitations on larger datasets, unlike simpler models.

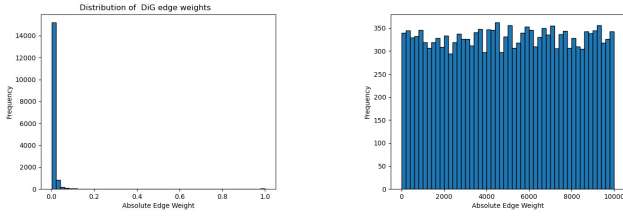
2) Explaining the Reason for Performance Differential

The performance variation stems from edge weight distributions. DiGCN(ib) produces a bimodal distribution peaked at 0 and 1 (Figure 4), while **RiG** shows uniform distribution. Experiments with structured random weights (Figure 5) show two-peak distributions perform poorly (accuracy: 36.5 ± 4.0), while three-peak distributions achieve better results (72.6 ± 4.9), exceeding DiGCN. This indicates weight distribution structure significantly impacts model effectiveness.

B. Hermitian GNNs

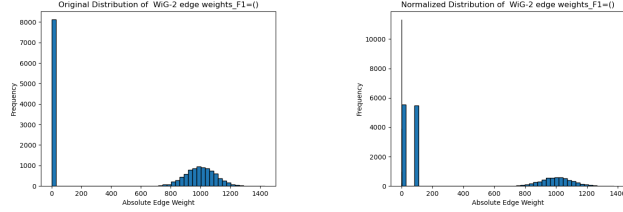
Not only do digraph inception models, but another popular branch of GNNs for directed graphs, Hermitian models, also suffer from unnecessary complexity. We will now prove this.

As MagNet [7] pioneered the introduction of Hermitian matrices in graph learning, we focus our analysis on this foundational work. In this section, we prove that MagNet is mathematically equivalent to GraphSAGE [2] with incidence



(a) Accuracy with edge weights generated by DiGCN(ib): 67.4 ± 8.1 (b) Accuracy with randomly generated edge weights: 85.2 ± 2.5

Fig. 4: DiG VS. RiG



(a) Accuracy with randomly generated edge weights (2 peaks): 36.5 ± 4.0 (b) Accuracy with randomly generated edge weights (3 peaks): 72.6 ± 4.9

Fig. 5: Random edge weights

normalization. This equivalence reveals that the apparent complexity of Hermitian-based approaches may not offer fundamental advantages over simpler methods.

For directed graphs, the adjacency matrix A differs from its transpose A^T . MagNet [7] uses $A_s = (A + A^T)/2$ to obtain a symmetric adjacency matrix, which is then incidence-normalized to \tilde{A}_s . Using a phase angle to distribute weight between real and imaginary parts, $\Theta = e^{2\pi qj(A-A^T)}$, the adjacency matrix becomes:

$$\begin{aligned} \hat{A}_s &= \tilde{A}_s \odot \Theta = \tilde{A}_s \odot e^{2\pi qj(A-A^T)} \\ &= \tilde{A}_s \odot \cos(2\pi q(A-A^T)) + j\tilde{A}_s \odot \sin(2\pi q(A-A^T)) \\ &= \hat{A}_s(\text{real}) + j\hat{A}_s(\text{imag}) \end{aligned}$$

where \odot denote component-wise multiplication, and the values of $\hat{A}_s(\text{real})$ and $\hat{A}_s(\text{imag})$ in various cases of edge directions are enumerated in Table VIII. As shown in Table VIII, $\hat{A}_s(\text{real})$ and $\hat{A}_s(\text{imag})$ are either $\cos \alpha$, $\sin \alpha$, or 0 or 1. As a result, $\hat{A}_s(\text{real})$ is a real symmetric matrix \bar{A}_s similar to \tilde{A}_s but the element where unidirectional edges the value is $\cos \alpha$ times the value in \tilde{A}_s . $\hat{A}_s(\text{imag})$ is a skew-symmetric matrix:

$$\hat{A}_s(\text{imag}) = 0.5 \sin(\alpha) D^{-\frac{1}{2}} (A - A^T) D^{-\frac{1}{2}}, \quad (14)$$

where D is the degree matrix of the graph.

In the end, they concatenate real and imaginary parts. Thus, the total output would be:

$$\text{Out}(\text{total}) = W_1 Z(\text{real}) + W_2 Z(\text{imag})$$

Specifically, they define the node feature as $\tilde{X} = X + jX$. When trying to follow ChebNet [36], MagNet made a coding

MagNet($\alpha = 2\pi q$)					
Edges	A_s	\tilde{A}_s	\hat{A}_s	$\hat{A}_s(\text{real})$	$\hat{A}_s(\text{imag})$
$m \rightarrow n$	0.5	$\frac{0.5}{d}$	$\frac{0.5}{d} e^{2\pi q \cdot j}$	$\frac{0.5}{d} \cos \alpha$	$\frac{0.5}{d} \sin \alpha$
$n \rightarrow m$	0.5	$\frac{0.5}{d}$	$\frac{0.5}{d} e^{-2\pi q \cdot j}$	$\frac{0.5}{d} \cos \alpha$	$-\frac{0.5}{d} \sin \alpha$
$m \leftrightarrow n$	1	d^{-1}	d^{-1}	d^{-1}	0
$m \not\leftrightarrow n$	0	0	0	0	0

TABLE VIII: Case enumeration of the elements in adjacency matrices for different edge types. Here, $A_s = 0.5(A + A^T)$ is the symmetrized adjacency matrix, \tilde{A}_s is the incidence-normalized adjacency matrix, and \hat{A}_s is the complex-valued adjacency matrix for MagNet with parameter $\alpha = 2\pi q$. The variable d denotes the node degree.

mistake in obtaining the Laplacian. They redundantly subtracted I for $L = I - \hat{A}_s$. Thus their $\hat{L} = I - \hat{A}_s - I = -\hat{A}_s$, and they mistakenly get:

$$\hat{T}_{k+2} = 2\hat{L}T_{k+1} - T_k$$

where T_1 is I while their T_2 is mistakenly $-\hat{A}_s$:

$$\hat{T}_2 = -\hat{A}_s$$

- When $K = 1$, the Hermitian output is:

$$\begin{aligned} Z_1 &= W_1 \hat{X} T_1 \\ &= W_1 (X + jX)(I + j0) = W_1 (X + jX) \end{aligned} \quad (15)$$

- When $K = 2$, with two weight matrices W_1 and W_2 , the Hermitian output is:

$$\begin{aligned} Z_2 &= Z_1 + W_2 (X + jX)(\hat{T}_2(\text{real}) + j\hat{T}_2(\text{imag})) \\ &= Z_1 + W_2 (X + jX)(-\hat{A}_s(\text{real}) - j\hat{A}_s(\text{imag})) \\ &= W_1 X + W_2 \hat{A}_s(\text{imag}) X - W_2 X \hat{A}_s(\text{real}) \\ &\quad + j(W_1 X - W_2 \hat{A}_s(\text{real}) X - W_2 \hat{A}_s(\text{imag}) X) \end{aligned} \quad (16)$$

Given that \hat{T}_k is linear combinations of \hat{A}_s up to the k -th power, and concatenating real and imaginary parts of the Hermitian output, the total output for different values of k becomes:

- For $k = 1$: Based on Equation 15, we get the total output:

$$\begin{aligned} \text{Out}_1(\text{total}) &= W_1 Z_1(\text{real}) + W_2 Z_1(\text{imag}) \\ &= W_1 X + W_2 X \end{aligned} \quad (17)$$

- For $k = 2$: Based on Equation 16, we get:

$$\begin{aligned} \text{Out}_2(\text{total}) &= W_3 Z_2(\text{real}) + W_4 Z_2(\text{imag}) \\ &= \hat{W}_1 X + \hat{W}_2 \hat{A}_s(\text{real}) + \hat{W}_3 \hat{A}_s(\text{imag}) \end{aligned} \quad (18)$$

According to Equation 14, Equation 18 can further be simplified to :

$$\begin{aligned} \text{Out}_2(\text{total}) &= W_1 X + W_2 D^{-\frac{1}{2}} \bar{A}_s D^{-\frac{1}{2}} X \\ &\quad + 0.5 \sin \alpha W_3 D^{-\frac{1}{2}} (A - A^T) D^{-\frac{1}{2}} X \end{aligned} \quad (19)$$

As layer-wise propagation of GraphSAGE is $W_1 X + W_2 A X$, the first two terms of Equation 19 are equivalent to GraphSAGE with incidence normalization. The third term of Equation 19 computes the difference between the sum of features from in-neighbors and out-neighbors. This information provides little help in node classification as MagNet performs

Norm.	GCN	DiG	DiGib	liG	liG12
Incidence	91.2±5.5	83.4±3.9	62.0±6.7	91.8±3.8	87.0±8.1
None	81.0±8.6	78.8±4.7	62.0±7.7	85.4±4.3	85.8±5.0

TABLE IX: Comparative analysis of model performance with and without incidence normalization. Results are reported as classification accuracy (%) with mean±standard deviation across 10 random splits using 4-layer architectures. For fair comparison, DiG and DiGib models were implemented without self-loops.

poorly on heterophilic graphs, thus $\sin \alpha$ should be 0 or close to 0 for better performance.

This analysis explains why MagNet’s performance is similar to GraphSAGE. The only effective difference is that in MagNet, its adjacency matrix A_s is normalized, while GraphSAGE has no normalization tricks, which explains why MagNet only outperforms GraphSAGE in the Telegram dataset [7], which is highly sensitive to normalization. The performance of various GNNs on Telegram dataset with or without incidence normalization is shown in Table IX. Without coding mistakes or using these tricks, the performance of MagNet would be the same as ChebNet, which is worse than GraphSAGE in most cases.

IX. CONCLUSIONS

We have addressed two critical challenges in Graph Neural Networks: the lack of theoretical support for invariance learning and the absence of a unified model for homophilic and heterophilic graphs. Our work establishes the theoretical foundation of **scale invariance** in graph learning and introduces **ScaleNet**, a unified network architecture that effectively leverages multi-scaled graphs and adaptive self-loops to dynamically handle diverse graph structures.

Through rigorous theoretical analysis, we demonstrate equivalence between Hermitian Laplacian methods and GraphSAGE with incidence normalization and propose efficient alternatives to computationally expensive edge weights in digraph inception networks. Experimental results on six benchmark datasets confirm that ScaleNet achieves state-of-the-art performance across both homophilic and heterophilic graphs while also demonstrating superior robustness to data imbalance.

Our contributions advance the theoretical understanding and practical application of GNNs, offering a unified, efficient, and adaptable framework for graph learning.

A limitation of our approach is the computational overhead introduced by the grid search required to select the optimal combination of multi-scaled graphs.

REFERENCES

[1] V. Gligorijević, P. D. Renfrew, T. Kosciolk, J. K. Leman, D. Berenberg, T. Vatanen, C. Chandler, B. C. Taylor, I. M. Fisk, H. Vlamakis, R. J. Xavier, R. Knight, K. Cho, and R. Bonneau, “Structure-based protein function prediction using graph convolutional networks,” *Nature Com-*

munications, vol. 12, p. 3168, May 2021. Publisher: Nature Publishing Group.

[2] W. Hamilton, Z. Ying, and J. Leskovec, “Inductive representation learning on large graphs,” *Advances in neural information processing systems*, vol. 30, 2017.

[3] R. Ying, R. He, K. Chen, P. Eksombatchai, W. L. Hamilton, and J. Leskovec, “Graph Convolutional Neural Networks for Web-Scale Recommender Systems,” in *Proceedings of the 24th ACM SIGKDD International Conference on Knowledge Discovery & Data Mining*, KDD ’18, (New York, NY, USA), pp. 974–983, Association for Computing Machinery, July 2018.

[4] T. N. Kipf and M. Welling, “Semi-supervised classification with graph convolutional networks,” *arXiv preprint arXiv:1609.02907*, 2016.

[5] Z. Tong, Y. Liang, C. Sun, X. Li, D. Rosenblum, and A. Lim, “Digraph inception convolutional networks,” *Advances in neural information processing systems*, vol. 33, pp. 17907–17918, 2020.

[6] E. Rossi, B. Charpentier, F. Di Giovanni, F. Frasca, S. Gunnemann, and M. M. Bronstein, “Edge directionality improves learning on heterophilic graphs,” in *Learning on Graphs Conference*, pp. 25–1, PMLR, 2024.

[7] X. Zhang, Y. He, N. Brugnone, M. Perlmutter, and M. Hirn, “Magnet: A neural network for directed graphs,” *Advances in neural information processing systems*, vol. 34, pp. 27003–27015, 2021.

[8] Q. Wu, H. Zhang, J. Yan, and D. Wipf, “Handling distribution shifts on graphs: An invariance perspective,” *arXiv preprint arXiv:2202.02466*, 2022.

[9] J. Sokolic, R. Giryes, G. Sapiro, and M. Rodrigues, “Generalization Error of Invariant Classifiers,” in *Proceedings of the 20th International Conference on Artificial Intelligence and Statistics*, pp. 1094–1103, PMLR, Apr. 2017. ISSN: 2640-3498.

[10] T. S. Cohen and M. Welling, “Group equivariant convolutional networks,” in *Proceedings of the 33rd International Conference on Machine Learning (ICML)*, vol. 48, pp. 2990–2999, PMLR, 2016.

[11] K. Lenc and A. Vedaldi, “Understanding image representations by measuring their equivariance and equivalence,” in *Proceedings of the IEEE conference on computer vision and pattern recognition*, pp. 991–999, 2015.

[12] X. Xie, Y. Sun, Y. Liu, M. Zhang, and K. C. Tan, “Architecture augmentation for performance predictor via graph isomorphism,” *IEEE Transactions on Cybernetics*, vol. 54, no. 3, pp. 1828–1840, 2023.

[13] V. Garg, S. Jegelka, and T. Jaakkola, “Generalization and Representational Limits of Graph Neural Networks,” in *Proceedings of the 37th International Conference on Machine Learning*, pp. 3419–3430, PMLR, Nov. 2020. ISSN: 2640-3498.

[14] S. Verma and Z.-L. Zhang, “Stability and generalization of graph convolutional neural networks,” in *Proceedings of the 25th ACM SIGKDD International Conference on Knowledge Discovery & Data Mining*, pp. 1539–1548, 2019.

[15] H. Maron, H. Ben-Hamu, N. Shami, and Y. Lipman, “Invariant and equivariant graph networks,” *arXiv preprint arXiv:1812.09902*, 2018.

[16] Y. Sui, Q. Wu, J. Wu, Q. Cui, L. Li, J. Zhou, X. Wang, and X. He, “Unleashing the Power of Graph Data Augmentation on Covariate Distribution Shift,” *Advances in Neural Information Processing Systems*, vol. 36, pp. 18109–18131, Dec. 2023.

[17] Y. Chen, Y. Bian, K. Zhou, B. Xie, B. Han, and J. Cheng, “Does Invariant Graph Learning via Environment Augmentation Learn Invariance?,” *Advances in Neural Information Processing Systems*, vol. 36, pp. 71486–71519, Dec. 2023.

[18] Y. You, T. Chen, Y. Sui, T. Chen, Z. Wang, and Y. Shen, “Graph contrastive learning with augmentations,” *Advances in neural information processing systems*, vol. 33, pp. 5812–5823, 2020.

[19] S. Suresh, P. Li, C. Hao, and J. Neville, “Adversarial Graph Augmentation to Improve Graph Contrastive Learning,” in *Advances in Neural Information Processing Systems*, vol. 34, pp. 15920–15933, Curran Associates, Inc., 2021.

[20] H. Sun, X. Li, Z. Wu, D. Su, R.-H. Li, and G. Wang, “Breaking the entanglement of homophily and heterophily in semi-supervised node classification,” in *2024 IEEE 40th International Conference on Data Engineering (ICDE)*, pp. 2379–2392, IEEE, 2024.

[21] M. Hashemi, S. Gong, J. Ni, W. Fan, B. A. Prakash, and W. Jin, “A comprehensive survey on graph reduction: Sparsification, coarsening, and condensation,” *arXiv preprint arXiv:2402.03358*, 2024.

[22] X. Gao, W. Dai, C. Li, H. Xiong, and P. Frossard, “Graph pooling with node proximity for hierarchical representation learning,” *arXiv preprint arXiv:2006.11118*, 2020.

- [23] J. Liang, S. Gurukar, and S. Parthasarathy, "MILE: A Multi-Level Framework for Scalable Graph Embedding," *Proceedings of the International AAAI Conference on Web and Social Media*, vol. 15, pp. 361–372, May 2021.
- [24] J. Gao and J. Wu, "Multiple sparse graphs condensation," *Knowledge-Based Systems*, vol. 278, p. 110904, Oct. 2023.
- [25] S. Abu-El-Haija, B. Perozzi, A. Kapoor, N. Alipourfard, K. Lerman, H. Harutyunyan, G. V. Steeg, and A. Galstyan, "MixHop: Higher-Order Graph Convolutional Architectures via Sparsified Neighborhood Mixing," in *Proceedings of the 36th International Conference on Machine Learning*, pp. 21–29, PMLR, May 2019. ISSN: 2640-3498.
- [26] D. Berberidis, A. N. Nikolakopoulos, and G. B. Giannakis, "Adaptive Diffusions for Scalable Learning Over Graphs," *IEEE Transactions on Signal Processing*, vol. 67, pp. 1307–1321, Mar. 2019.
- [27] E. Chien, J. Peng, P. Li, and O. Milenkovic, "Adaptive universal generalized pagerank graph neural network," *arXiv preprint arXiv:2006.07988*, 2020.
- [28] J. Zhu, Y. Yan, L. Zhao, M. Heimann, L. Akoglu, and D. Koutra, "Beyond homophily in graph neural networks: Current limitations and effective designs," *Advances in neural information processing systems*, vol. 33, pp. 7793–7804, 2020.
- [29] R. Zhang, Z. Chen, T. Xiao, Y. Wang, and K. Kuang, "Discovering invariant neighborhood patterns for heterophilic graphs," *arXiv preprint arXiv:2403.10572*, 2024.
- [30] Z. Tong, Y. Liang, C. Sun, D. S. Rosenblum, and A. Lim, "Directed graph convolutional network," *arXiv preprint arXiv:2004.13970*, 2020.
- [31] N. Alvarez-Gonzalez, A. Kaltenbrunner, and V. Gómez, "Beyond Weisfeiler–Lehman with Local Ego-Network Encodings," *Machine Learning and Knowledge Extraction*, vol. 5, pp. 1234–1265, Dec. 2023.
- [32] P. Veličković, G. Cucurull, A. Casanova, A. Romero, P. Liò, and Y. Bengio, "Graph attention networks," in *International Conference on Learning Representations*, 2018.
- [33] K. Xu, C. Li, Y. Tian, T. Sonobe, K.-i. Kawarabayashi, and S. Jegelka, "Representation learning on graphs with jumping knowledge networks," in *International conference on machine learning*, pp. 5453–5462, PMLR, 2018.
- [34] Y. Hu, H. You, Z. Wang, Z. Wang, E. Zhou, and Y. Gao, "Graph-MLP: Node Classification without Message Passing in Graph," June 2021. arXiv:2106.04051 [cs].
- [35] J. Gasteiger, A. Bojchevski, and S. Günnemann, "Predict then Propagate: Graph Neural Networks meet Personalized PageRank," Apr. 2022. arXiv:1810.05997 [cs, stat].
- [36] M. Defferrard, X. Bresson, and P. Vandergheynst, "Convolutional Neural Networks on Graphs with Fast Localized Spectral Filtering," in *Advances in Neural Information Processing Systems*, vol. 29, Curran Associates, Inc., 2016.
- [37] F. Monti, K. Otness, and M. M. Bronstein, "MOTIFNET: A motif-based graph convolutional network for directed graphs," in *2018 IEEE Data Science Workshop (DSW)*, (Lausanne, Switzerland), pp. 225–228, IEEE, June 2018.
- [38] Y. Ma, J. Hao, Y. Yang, H. Li, J. Jin, and G. Chen, "Spectral-based graph convolutional network for directed graphs," *arXiv preprint arXiv:1907.08990*, 2019.
- [39] G. Kollias, V. Kalantzis, T. Ide, A. Lozano, and N. Abe, "Directed Graph Auto-Encoders," *Proceedings of the AAAI Conference on Artificial Intelligence*, vol. 36, pp. 7211–7219, June 2022.
- [40] S. Fiorini, S. Coniglio, M. Ciavotta, and E. Messina, "Sigmanet: One laplacian to rule them all," in *Proceedings of the AAAI Conference on Artificial Intelligence*, vol. 37, pp. 7568–7576, 2023.
- [41] Y. He, M. Perlmutter, G. Reinert, and M. Cucuringu, "MSGNN: A Spectral Graph Neural Network Based on a Novel Magnetic Signed Laplacian," in *Proceedings of the First Learning on Graphs Conference*, pp. 40:1–40:39, PMLR, Dec. 2022.
- [42] S. Fiorini, S. Coniglio, M. Ciavotta, and E. Messina, "Graph learning in 4d: A quaternion-valued laplacian to enhance spectral gens," in *Proceedings of the AAAI Conference on Artificial Intelligence*, vol. 38, pp. 12006–12015, 2024.
- [43] W. Zhuo and G. Tan, "Commutate graph neural networks," *arXiv preprint arXiv:2407.01635*, 2024.